Power-law exponents and hidden bulk relation in the impedance spectroscopy of solids *

J. Ross Macdonald

Department of Physics and Astronomy, University of North Carolina, Chapel Hill, NC 27599-3255, (USA)

(Received 10 January 1994; in revised form 17 March 1994)

Abstract

Several aspects of the bulk response of disordered solids are investigated. The question is explored of how constant loss at the dielectric level, equivalent to the real part of the admittance being proportional to frequency, can occur. Such response is found to be possible for dielectric system response but is not likely for conducting system response. This kind of dielectric system behavior, which arises from the presence of a flat-top box probability distribution of activation energies, is further used to investigate and illustrate a promising alternative to Kronig–Kramers transformation of small-signal ac response data. For conducting system relaxation, the response of a possibly quite general dispersion equation, the Bryksin–Dyre–Macdonald (BDM) equation, an effective-medium approximation, is explored and used to illustrate how the underlying bulk dispersion of a material is obscured or hidden within the usual high frequency bulk semicircle present in impedance-level complex plane plots.

1. Introduction

There are several areas of current interest in impedance spectroscopy (IS) data analysis. They are interesting because they involve new possibilities, limitations and partly unsolved problems. As such, they provide stimuli for the future work needed to solve some of the problems and to explore the new possibilities and limitations.

Three of these areas are defined by the following proposals: (a) many electrically conducting ionic crystals and glasses exhibit a constant ac loss per cycle independent of frequency at relatively low temperatures, so that the response requires that the real part of the ac admittance or conductivity is exactly proportional to frequency, termed a "new universality" [1,2]; (b) there is a single universal relaxation equation describing conducting system relaxation response at sufficiently low temperatures [3]; (c) the relaxation response of many disordered solids arises solely (1) from a dc conductivity and unrelated dielectric (e.g. dipolar) dispersion [4–6] or, alternatively, (2) from conducting system dispersion with no significant dielectric dispersion in the measurement range [4,5,7] or, most generally, (3) from a combination of conducting system and dielectric system dispersion [8–10]. Note that these three propositions are independent and are not necessarily related to each other or mutually consistent for a given class of materials.

It will not have escaped the reader's notice that these various response possibilities all deal with bulk effects in solids and ignore electrode and interface effects, often those of dominant interest in electrolyte studies. Figure 1 shows a plausible equivalent circuit which can accommodate a considerable range of experimentally observed response behavior which includes both types of effects. The left-hand section, which involves the arbitrary distributed circuit element DE3 [11], is included to represent the intensive electrode/interface effects present, and the right-hand section is proposed to account for general bulk response.

In many IS experiments, it is found sufficient to represent the bulk response by the parallel combination of the frequency-independent ideal circuit elements R_∞ and C_∞, and when R_∞ is small compared with other resistances in the system the effects of R_∞ and C_∞ are often unmeasured and/or ignored. R_∞ is the bulk or solution resistance of the system (some-

* In honour of Professor Richard P. Buck on the occasion of his 65th birthday.

0022-0728/94/$7.00
SSDI 0022-0728(94)03520-D

times written as R_B or R_S), and C_∞ is the bulk or geometrical cell capacitance (otherwise written as C_B or C_g). In the ideal case, their presence leads to a semicircle in the impedance complex plane, but when the intensive time constant $\tau_\infty \equiv R_\infty C_\infty$, the dielectric relaxation time, is sufficiently small, part or none of the semicircle will appear within the experimentally available frequency range.

Nevertheless, one should consider the possibility that both the conducting system response, associated with percolating charges, and the dielectric system response, often arising from dipole rotation, involve frequency-dependent relaxation processes represented by the distributed circuit elements DEC (conducting system) and DED (dielectric system) shown in Fig. 1 [8–10] (case (c3) above). Although, as will be shown herein, these effects, which are virtually always present in some (possibly very high) frequency range, are usually obscured or completely hidden, it is possible in principle and in practice, at least for high resistivity materials [7,10], to uncover their secrets and learn more about the detailed response of the material observed.

Richard P. Buck was one of the early pioneers in the area of impedance measurements and interpretation [12,13]. As such, it is appropriate that the present work involves such matters. Further, over the years Buck and his associates [14,15] and others [16–19] have devoted appreciable effort towards the elucidation of bulk response in IS. Therefore we shall deal here only with such bulk response, as represented by the right-hand part of Fig. 1, and will attempt to relate the results, at least in part, to the three areas mentioned above.

The impedance of the bulk section of the circuit of Fig. 1 can be written as

$$\begin{aligned} Z(\omega) &\equiv [Y(\omega)]^{-1} \equiv [Y_C(\omega) + Y_D(\omega)]^{-1} \\ &\equiv \Big\{ [Z'_C(\infty) + \Delta Z'_C I_C(\omega)]^{-1} \\ &\quad + i\omega[C_D(\infty) + \Delta C'_D I_D(\omega)] \Big\}^{-1} \end{aligned} \tag{1}$$

where subscripts C and D indicate conducting and dielectric system contributions respectively. Further, $\Delta Z'_C \equiv Z'_C(0) - Z'_C(\infty)$, $Z'_C(0) = R_{dc}$, where R_{dc} is the dc resistance for this model, $Z'_C(\infty) = R_\infty$ when $\Delta Z'_C = 0$ and we can set $\Delta Z'_C = R_\infty$ when $Z'_C(\infty) = 0$ and $I_C(\omega) \approx 1$ within the available frequency range. Likewise, $\Delta C'_D \equiv C'_D(0) - C'_D(\infty)$, $C'_D(0) = C_{dc}$, where C_{dc} is the dc capacitance for this model, and $C'_D(\infty) = C_\infty$. Here $C_D(\omega) \equiv C'_D(\omega) - iC''_D(\omega)$ is the complex dielectric system capacitance and is equal to $\epsilon_D(\omega)C_c$, where $\epsilon_D(\omega)$ is the complex dielectric constant of the dielectric system and C_c is the capacitance of the empty measuring cell.

The quantities I_C and I_D are normalized relaxation response functions which are unity at $\omega = 0$ and zero at $\omega = \infty$. They are discussed in the Appendix for several situations of interest such as the conducting system Bryksin–Dyre–Macdonald (BDM) equation [3,10,20,21], the box distribution of relaxation times for dielectric systems ($\phi_D = 0$) [22,23] and the box distribution of activation energies for conducting systems ($\phi_C = 1$) [23–26]. Here ϕ is a characteristic parameter of

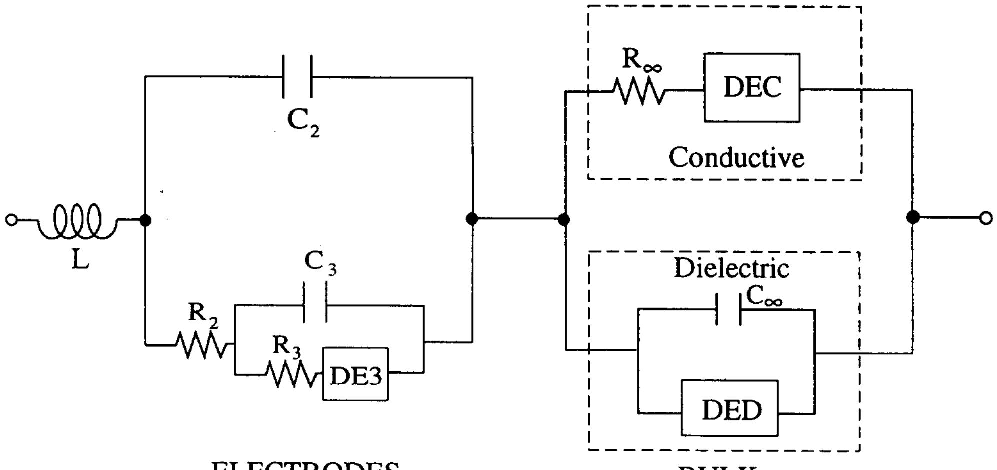

Fig. 1. An equivalent circuit implemented in the complex nonlinear least-squares fitting program LEVM which can be used for fitting of small-signal ac response data. DE3, DEC and DED are arbitrary distributed circuit elements which cannot necessarily be represented by a finite number of ideal circuit elements such as resistances and capacitances.

the exponential distribution of activation energies (EDAE) response (see Appendix). Note that it is necessary to distinguish between the full complex dielectric constant $\epsilon(\omega)$ and $\epsilon_D(\omega)$ in case (c3) because then the conducting system contributes its own dielectric increment to $\epsilon(\omega)$ [7,10].

The above definitions show that case (c1) occurs when $\Delta Z'_C = 0$, (c2) when $\Delta C'_D = 0$ and (c3) when neither is zero. In the following, cases (a), (b) and (c2) [3,7,20] will be particularly considered, although some work also exists on more complicated case (c3) situations [6,8,10].

2. Constant-loss response

In order to investigate the ac loss at the dielectric level, one must first subtract $Y'_C(0) \equiv [Z'_C(0)]^{-1}$, if it is nonzero, from $Y'(\omega)$ and then divide the result $\Delta Y'(\omega)$ by ωC_c to obtain $\Delta\epsilon''(\omega)$. In refs. 1 and 2, it is this quantity that has been stated to be frequency-independent and thus illustrative of a "new universality", even up to room temperature for some materials. But there is always unavoidable error in the estimate of $Y'_C(0)$, which is magnified by the subtraction process, and the results are usually shown at either the Y or the ϵ immittance level as log–log plots, reducing apparent variation appreciably [7,25,26]. Detailed analyses [7,10] of data for single-crystal NaCl [1] and Al^{3+}-doped $CaTiO_3$ ceramic material [2] strongly indicate that $\Delta\epsilon''(\omega)$ is not, in fact, exactly constant over any appreciable frequency region, but its approximate constancy at low temperatures arises from a combination of conducting and dielectric system responses.

In general, $\Delta Y'(\omega)$ can be expressed as proportional to $\omega^{s(\omega)}$, where the power-law exponent $s(\omega)$ is the slope of a log–log plot of $\Delta Y'(\omega)$ vs. ω. For constant loss, $s(\omega) = 1$, independent of frequency (at least over an appreciable frequency range). There has been considerable discussion of $s(\omega)$ in the literature for conducting systems, and, contrary to the results of refs. 1 and 2, it is usually found only to approach unity from below as the temperature becomes very low. Such behavior follows from both an EDAE model [23,24] and the BDM response equation [10,20]. In fact, both models lead to a frequency-dependent $s(\omega)$ which approaches unity logarithmically in frequency at high relative frequencies and only reaches it at infinite frequency [3,21,25]. Thus it seems unlikely that conducting system dispersion alone can lead to constant-loss behavior except in this limit.

But there is a way to obtain very nearly constant loss over an extended frequency range at reasonable temperatures and frequencies. It is a dielectric response phenomenon, not a conductive system phenomenon.

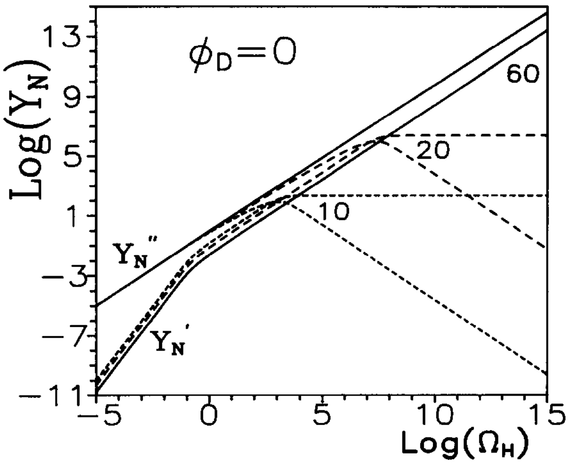

Fig. 2. Log–log response of normalized admittance components vs. normalized frequency Ω_H for dielectric response calculated for a flat-top box (e.g. uniform) distribution of activation energies: $\phi_D = 0$. The numbers 10, 20, and 60 are cut-off values of x_H, the maximum activation energy of the distribution in normalized form.

Constant loss only appears when there is a flat-top activation energy probability distribution present which is associated with the value $\phi_D = 0$ [9,23]. Then, all transition rates within an allowed range are equally probable. Because there is a large body of literature which strongly suggests, and often claims, that constant loss is indeed present for a wide variety of solids at low but nonzero temperatures, the question of the provenance of such a loss, if it is actually present, is particularly important, and therefore it and some of its associated response will be addressed in some detail herein.

Wang and Bates [27] have presented a theoretical model of localized hopping in a potential double well which leads to dielectric response with $\phi_D = 0$ or $\phi_D \neq 0$. In the next few figures some of the possible responses arising from the $\phi_D = 0$ choice are explored. All the curves of the graphs of the present work were calculated using the readily available LEVM V.6.1 complex nonlinear least-squares fitting (CNLSF) program either to generate data from a model or to fit it to a model [28,29]. [1] LEVM now includes both the EDAE response model and the BDM conducting system equation expressed as a distributed-circuit element.

[1] The LEVM program V.6.1 is comprehensive and includes many powerful features for accurate fitting of conducting and dielectric system frequency and time responsible data. Except where otherwise stated, all present fits with LEVM used proportional or functional-proportional weighting.

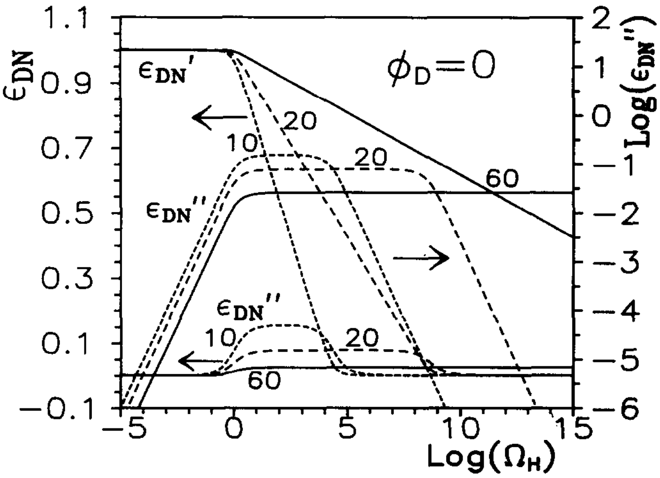

Fig. 3. Normalized dielectric level response ϵ_{DN} vs. log normalized frequency calculated from the results of Fig. 2. Here ϵ_{DN}'' curves are shown on a linear scale (left) and a log scale (right). Note the linear dependence of parts of the ϵ_{DN}' curves on $\log(\Omega_H)$.

2.1. Exact dielectric system model response

Figure 2 shows the log–log normalized admittance response of the $\phi_D = 0$ EDAE model over an extremely large normalized frequency range. Here $Y_C(\omega) = 0$ for all ω. The EDAE box model involves a flat-top activation energy probability density extending from zero activation energy to a maximum value of E_H. In the figure, the numbers 10, 20 and 60 are values of the normalized upper cut-off, $x_H \equiv E_H/k_BT$. For example, if $E_H \approx 1.034$ eV and $T = 300$ K, $x_H \approx 40$. Although this log–log plot shows some regions of constant slope, that of $Y_N''(\equiv Y_{DN}'')$ is particularly deceiving. On calculating and plotting the corresponding ϵ_{DN}', here defined as Y_N''/Ω_H, and ϵ_{DN}'' quantities, one sees a different picture in Fig. 3, where ϵ_{DN}'' is plotted both linearly and logarithmically. The normalization used here is defined by $\epsilon_{DN}(\omega) \equiv \epsilon_D(\omega)/\Delta\epsilon_D'$. See the Appendix for some other definitions.

As expected, ϵ_{DN}'' is indeed constant over a large frequency range for $x_H \geqslant 20$, but it follows from eqn. (A5) that $\epsilon_{DN}' \approx 1 - x_H^{-1} \ln[1 + \Omega_H^2]^{1/2}$ for $\ln(\Omega_H) < x_H$. Thus the corresponding Y_N'' curve in Fig. 2 cannot have a constant slope in this region, a good example of how log–log plots with apparently constant slopes can lead to quite misleading conclusions. Figure 4 shows the Cole–Cole complex plane plot of the data of Figs. 2 and 3. Note the points of constant frequency shown on the three curves; the arrows show the direction of increasing frequency. These results confirm that, although the loss is not quite constant over any region for $x_H = 10$, it is very well approximated as constant for $x_H \geqslant 20$.

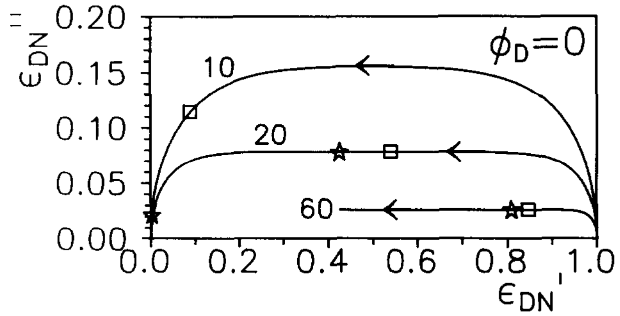

Fig. 4. Complex plane plot at the dielectric level of the full data of Figs. 2 and 3: □ located at $\Omega_H = 10^4$; ☆ located at 10^5. Arrows indicate the direction of increasing frequency. Note that, for clarity, the vertical scale units are larger than the horizontal scale units.

It is common [6,8,30,31] to examine high resistivity IS data from disordered solids by plotting small signal frequency response results at the complex modulus level, where $M \equiv 1/\epsilon$. Figure 5 shows such results for $\phi_D = 0$ and $x_H = 15$. Up to this point, the data plotted have implicitly involved the choice $\epsilon_{DN}'(\infty) = 0$, and so we have taken $\Delta\epsilon_{DN}' = \epsilon_{DN}'(0)$, but setting $\epsilon_{DN}'(\infty)$ to zero is physically unrealistic because even in the absence of any material $\epsilon_D'(\infty) = 1$. Figure 5 demonstrates the effect of $\epsilon_{DN}'(\infty)$ variation on the shape of M_{DN}'' response. There is no peak for the value $\epsilon_{DN}'(\infty) = 0$, and the curve continues to increase indefinitely proportionally to ω [20]. Thus it is clear that the commonly observed peaked response arises entirely from the presence of a nonzero value of $\epsilon_{DN}'(\infty)$. Further, note the asymmetry of the peaked curves, illustrative of a long low frequency tail. Incidentally, as ϕ_D approaches unity for fixed $\epsilon_{DN}'(\infty)$, the curves approach complete symmetry around their peaks.

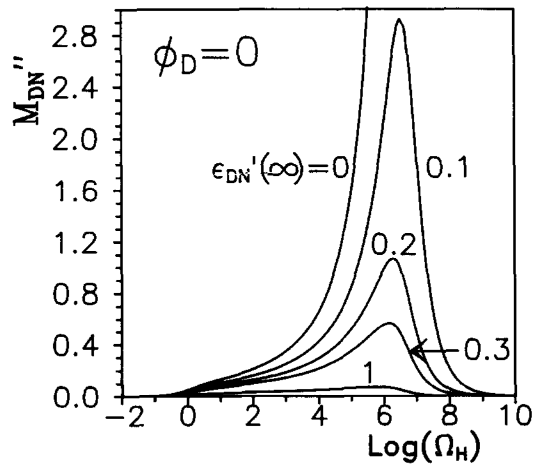

Fig. 5. Normalized complex modulus component M_{DN}'' vs. $\log(\Omega_H)$ for $x_H = 15$ and five values of $\epsilon_{DN}'(\infty)$, the normalized high frequency limit value of the dielectric constant.

Figure 6 shows the complex-plane modulus response for $\epsilon'_{DN}(\infty) = 0$ and $\epsilon'_{DN}(\infty) = 0.1$ for several values of x_H. The minimum value of M'_{DN}, at $\omega = 0$ is just $[1 + \epsilon'_{DN}(\infty)]^{-1}$ here since normalization leads to the value $\Delta\epsilon'_{DN} = 1$. Although the curves appear to be similar to those of the Cole–Davidson (CD) empirical model [9,11] or of the Kohlrausch–Williams–Watts [KWW] fitting model, both available as distributed-circuit elements in LEVM [11,28], it turns out that they cannot be fitted adequately with these models when $\phi_D = 0$.

2.2. *Distribution of relaxation time fitting: an alternative to Krönig–Kramers transformation*

The Krönig-Kramers (KK) integral transformation relations are found useful in IS to test whether data are well represented by a passive time-invariant system [32–34], and in many areas of physics and optics to predict the real or imaginary part of a complex response when only one of them is available. But since KK transformation requires integration from $\omega = 0$ to $\omega = \infty$, extrapolation outside the finite range of actual experimental data is always required and often leads to appreciable uncertainties. It is interesting to examine the transformation/fitting problem using some of the present $\phi_D = 0$ model data. To do so, the data were fitted, using LEVM, to a simple distribution of relaxation times model (DRT) which consists, for the present dielectric system, of N branches in parallel, each branch made up of a resistor and capacitor in series. Although this approach has long been known in the dielectric response area [35] without CNLSF, it has only recently been applied in IS as a "measurement model" fitting procedure to allow all $2N$ parameters of the fit to be free during fitting [7,20,36]. Such fitting can yield the N relaxation strengths p_i whose sum is automatically normalized to unity in the LEVM fit. These quantities and their corresponding time constants τ_i define a discrete normalized DRT associated with the data, which is the solution of an inverse (deconvolution) problem. For synthetic data, N can be increased to yield a unique fit with residuals as small as desired, although for experimental data there is a limit to the utility of increasing N.

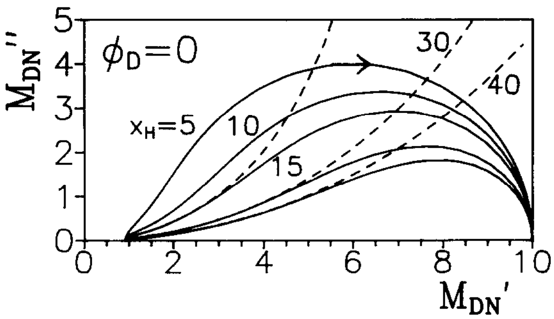

Fig. 6. Complex plane plot at the complex modulus level of $\phi_D = 0$ data for five values of x_H: ——— $\epsilon'_{DN}(\infty) = 0.1$; — — — $\epsilon'_{DN}(\infty) = 0$.

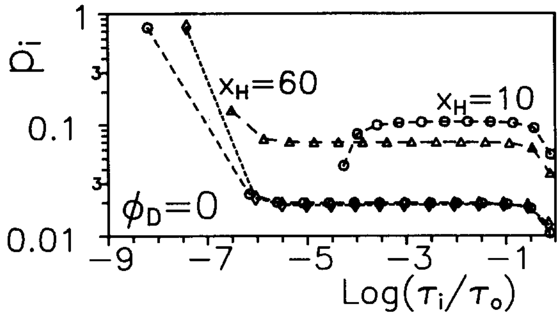

Fig. 7. Values of the discrete DRT normalized strength parameter p_i vs. $\log(\tau_i/\tau_o)$ for $\phi_D = 0$ and two values of x_H (the normalizing quantity τ_o is 1 s): — — — $x_H = 60$ curve resulting from the DRT fit of the full complex ϵ_{DN} data; --- $x_H = 60$ curve resulting from fitting the real part of the data; △ $x_H = 60$ curve arising from imaginary part fitting.

Figure 7 shows discrete DRTs for $x_H = 10$ and $x_H = 60$. Only the points are significant; the lines are included to guide the eye. The data fitted extended from $\Omega_H = 0.01$ to $\Omega_H = 2 \times 10^6$, and the standard deviation of the relative residuals of the fit for the $x_H = 10$ choice was less than 1.6×10^{-4} using $N = 11$ and 84 data points. For the $x_H = 60$ choice, $N = 14$ was used. Note that the $x_H = 60$ data are abruptly truncated with a cut-off at 2×10^6 Hz, while such a cut-off for $x_H = 10$ still covers nearly all the significant response (see Fig. 3). The $x_H = 10$ DRT shows a flat top and a shape much like that shown in Fig. 4 for the complex plane response. Although the $x_H = 60$ curves also show an extensive constant region, the abrupt cut-off at the high frequency end leads to a corresponding rise of p_i at small τ_i values. Essentially the same DRT results were obtained for $x_H = 10$ using either the full complex data or the real or imaginary part for fitting. But for $x_H = 60$, we see that the result for the imaginary-data fit is considerably different from those for the other two data choices.

Figure 8 shows the actual relative residuals r of the $x_H = 60$ full complex fit, which yielded a standard deviation estimate of the relative residuals of 5.1×10^{-4}. Those for the imaginary part of the data are clearly much larger than those for the real part over most of the range, but even the imaginary ones are all less than 0.001 in magnitude. The CNLS fit procedure levels the relative residuals as much as possible and produces a period of oscillation determined by the choice of N ($N - 1$ peaks of a single sign).

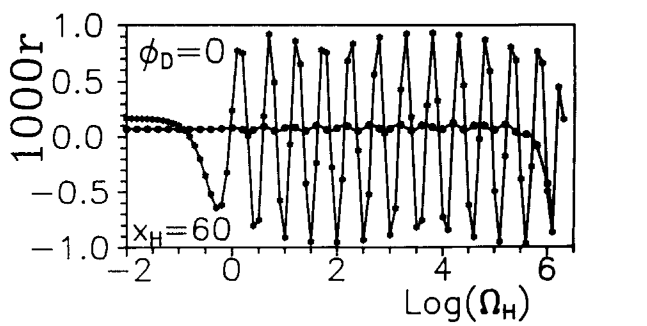

Fig. 8. The dependence on $\log(\Omega_H)$ of the relative residuals $r = r' + ir''$ of the DRT complex nonlinear least squares fit which led to the $x_H = 60$ results in Fig. 7. ○ real part residuals; * imaginary part residuals.

Figure 9 demonstrates how well DRT fitting can substitute for, and even improve on, KK predictions even in a difficult situation. The broken vertical line in Fig. 9 shows the extent of the data used to obtain DRT results. These results were then used to predict $\epsilon'_{DN}(\omega)$ and $\epsilon''_{DN}(\omega)$ over a range extending nearly three decades higher in frequency than the original fitted data. This allows one to observe just how the DRT fitting automatically extrapolates the real and imaginary response beyond the truncation point of the original data. Results for $x_H = 10$ are not shown because the fit results of the full complex data and the full $\epsilon_{DN}(\omega)$ predictions obtained from either real part or imaginary part fits were indistinguishable from the

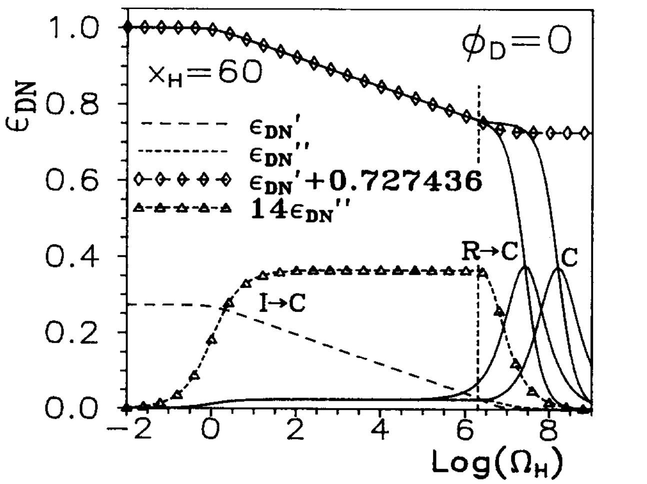

Fig. 9. Results of DRT fitting of ϵ_{DN} data extending up to the broken vertical dashed line and then truncated. The fitting model parameters have then been used to extrapolate the fits for nearly three further decades at the high frequency end. Curves are shown for the original fit of the complex data (C), for the fit of the ϵ'_{DN} data only with the results used to predict imaginary response (R → C) and for the fit of ϵ''_{DN} data with the results used to predict the real response (I → C).

original ϵ_{DN} data. In this case, the DRT alternative to KK transformation is essentially ideal.

Within the span of the original $x_H = 60$ data, the DRT fit of the full complex data (marked C in Fig. 9) yielded results indistinguishable from the data themselves, but the extended region at high frequencies shows how the branch with the smallest time constant dominated the response in this region. The DRT fit of the $\epsilon'_{DN}(\omega)$ data yields similar results but with a larger smallest time constant, as shown in Fig. 7. Results are quite different for the $\epsilon''_{DN}(\omega)$ DRT fit. The predicted $\epsilon''_{DN}(\omega)$ results agree with the input $\epsilon''_{DN}(\omega)$ data within their range but as shown on the curve with triangle symbols, which is expanded by a factor of 14 for clarity, the final decay shows no peak.

The $\epsilon'_{DN}(\omega)$ predictions, which come entirely from the imaginary part fit, are displaced by an amount of about 0.727 below the actual $\epsilon'_{DN}(\omega)$ input data but agree indistinguishably with them when this factor is added! Thus, although the predictions of the imaginary part from the real part only are excellent even in this extreme cut-off situation, the real part predicted from the imaginary part data requires the addition of a constant value, just as the corresponding KK relation at the ϵ level involves the addition of $\epsilon'_{DN}(\infty)$, a quantity not predictable from the imaginary data. The present and earlier [7,20] results thus suggest that, if one is satisfied with predictions of one part from the other within the range of the original data, the DRT method with an adequate value of N provides at least as good results as does KK transformation and does so with a much simpler procedure which does not require guessing what happens outside the finite range of the data.

Finally, Fig. 10 shows fitting results for a region of the $\phi_D = 0$ data with cut-offs at both ends obtained using the KWW fitting model [11,37]. Here the data are restricted to the approximately constant $\epsilon''_{DN}(\omega)$

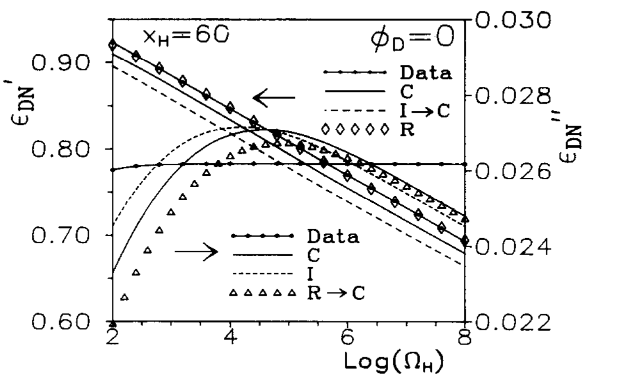

Fig. 10. KWW fits of the $x_H = 60$ data truncated at the extremes shown on the plot: ● original data are shown by the curves with small dots; the results of the various fits are identified on the figure.

region, and KWW fits were made using the complete complex data or its real or imaginary parts. The real or imaginary fit results were then used to predict the other part of the complex data. It is surprising how well the real part fit fitted the real data, but none of the fits could produce an entirely constant $\epsilon''_{DN}(\omega)$ response. This fitting led to an estimate of the KWW exponent parameter β of 0.093. Fitting with the CD empirical model [9,11,33] yielded a slightly worse fit, but an estimate of the CD exponent of about 0.02, in close agreement with the value of 0.021 obtained directly from the data at the Y level as follows. If one assumes (incorrectly) that both the real and imaginary lines have constant log–log slope, then in this region the constant-phase-angle distributed-circuit element [11,33] applies and agrees with the high frequency limiting response of both the KWW and CD models. In the middle frequency region of the x_H curves of Fig. 2, the ratio Y''_N/Y'_N is about 30.9, equal to $\tan(\pi\psi/2)$. This leads to $1-\psi \approx 0.021$, the equivalent log–log slope at the epsilon level. But of course the $\phi_D = 0$ data do not actually exhibit such a slope at this level.

3. Hidden aspects of bulk response

The information provided by estimates of R_∞ and C_∞ from experimental data can be useful in understanding something about the conduction and dielectric processes occurring in the measured material [14–19,38], but it does not exhaust what can potentially be learned from such data. We shall demonstrate this here by using a plausible, and perhaps very general, conducting system relaxation response equation, the BDM, first without any effect of $C_\infty \equiv \epsilon_D(\infty)C_c$ included, and then with it present. In this way one can observe what happens when the effects of C_∞, which are always present in experimental data, are subtracted from the data. Note that R_∞ and C_∞ do not form a KK-related dispersion pair.

The BDM [10,20] has a characteristic, virtually temperature independent, somewhat asymmetric shape, when its impedance predictions are plotted in normalized form in the complex plane. The solid line in Fig. 11 shows this response for the choice $x_c = 30$, where x_c is the normalized, effective maximum activation energy involved (see the Appendix for more details). In the following results, the normalization $Z_{CN}(\Omega_E) \equiv Z_C(\Omega_E)/\Delta Z'_C$ will usually be used for simplicity. Here Ω_E is the effective medium BDM normalized frequency defined in the Appendix. Incidentally, the characteristic complex plane arc shape of the BDM shown in Fig. 11 is quite similar to that following from the jump relaxation model of Funke [39] which involves non-random correlated hopping. Although the effective-medium approach leading to the BDM [20,25] does not explicitly include correlation and relaxation of the positions of neighboring mobile ions after a hop, its self-consistency requirement may cause it to take some implicit account of these effects.

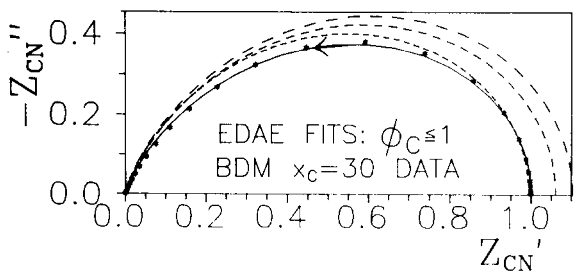

Fig. 11. Complex plane plot at the impedance level of normalized BDM data calculated with $x_C = 30$ and several EDAE fits with different weightings: PWT, data proportional weighting; UWT, unity weighting. The various fit lines and ϕ_C values are further identified on the next two figures, but here the estimated ϕ_C value for unity weighting with ϕ_C free to vary (---) is 0.828.

The other responses shown in Fig. 11 were obtained by fitting the BDM exact data with the EDAE model using different weighting possibilities. For a conducting system, this model yields maximum (but frequency-dependent) log–log slopes at the Y level for the choice $\phi_C = 1$ (the box distribution) and also involves frequency-dependent slopes for $\phi_C \neq 0$. We see that unity weighting yields a closer fit to the data shown than does proportional weighting, but a ϕ_C value of appreciably less than unity is required, which is less plausible than the estimate of 0.963 obtained with proportional weighting [20].

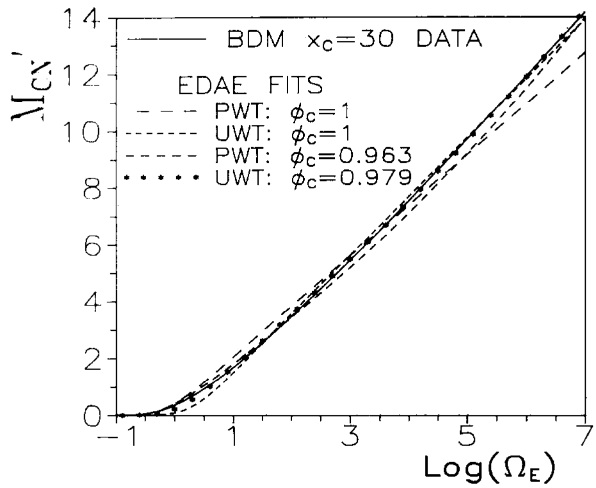

Fig. 12. M'_{CN} vs. $\log(\Omega_E)$ for BDM data and for the EDAE fits identified in the figure. Here Ω_E is the BDM effective-medium normalized frequency.

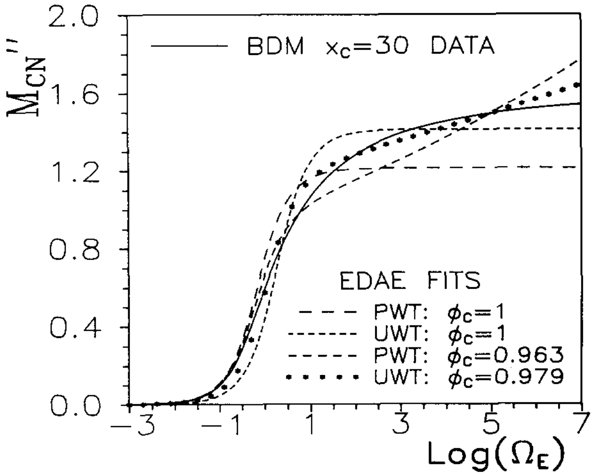

Fig. 13. M''_{CN} vs. $\log(\Omega_E)$ for BDM data and for the EDAE fits identified in the figure.

Figs. 12 and 13 show the corresponding results for the same data for M'_{CN} and M''_{CN}, respectively. The Z_{CN} and M_{CN} fit parameter estimates are the same for proportional weighting but differ for unity weighting. Although the M'_{CN} unity weight fit is again the best, there are considerable discrepancies between the data and any of the fits for M''_{CN}, which are certainly sufficiently large to allow one to distinguish between the two models for experimental data with even appreciable errors. But note that these results involve the choice $\epsilon'_D(\infty) = 0$. For experimental data, this quantity will be nonzero and its effect must be accounted for, as discussed in more detail later. Incidentally, although the choice of $\phi_C = 1$ leads to flat-top curves in the

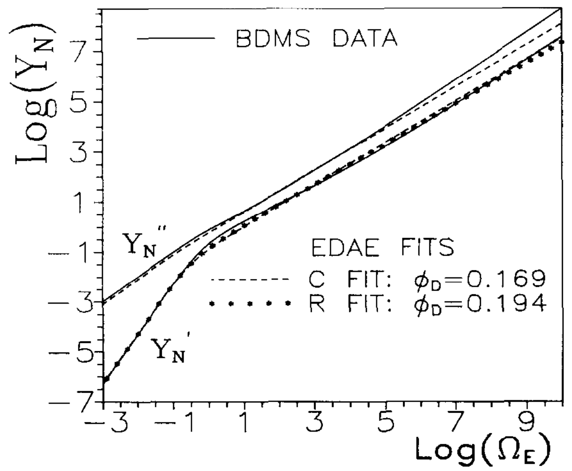

Fig. 14. Admittance level fits of BDMS data with the dc limiting value subtracted (BDMS) with the dielectric level EDAE model with $x_H = 60$. Complex data fits and fits of the real part only are plotted at the normalized admittance level.

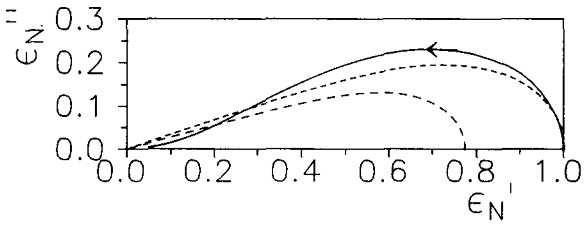

Fig. 15. Dielectric level complex-plane plots showing EDAE fits of BDMS data with PWT (— — —, $\phi_D \approx 0.169$) and UWT (---, $\phi_D \approx 0.204$).

modulus-level complex plane [26], like those shown in Fig. 4 at the ϵ level with the EDAE dielectric system choice $\phi_D = 0$ [23], the BDM does not yield such a flat top, as is shown by the results of Fig. 13 (see also ref. 20).

As well as the question of how well full BDM data can be approximated by the conducting system EDAE response model, it is worthwhile investigating the degree to which it can be approximated by the EDAE model at the dielectric level when its dc limit $Y'_C(0) = [Z'_C(0)]^{-1}$ is subtracted from the data (then identified as BDMS data). Here, this can be done exactly, but there is always some uncertainty in the proper value of $Y'_C(0)$ to subtract for experimental data. Figures 14–17 show what happens when this is done for low temperature BDM data calculated with $x_c \to \infty$. They indicate that, rather than $\phi_D = 0$, values near $\phi_D = 0.2$ are needed to obtain fairly good fits. Comparable results are obtained with the CD empirical fitting model. It is worth mentioning that for several different glasses Cole and Tombari [40] also found CD-like response of the present kind with CD exponents of the order of 0.35–0.40 and have remarked on the excess high frequency adsorption present [30]. They also found that the acti-

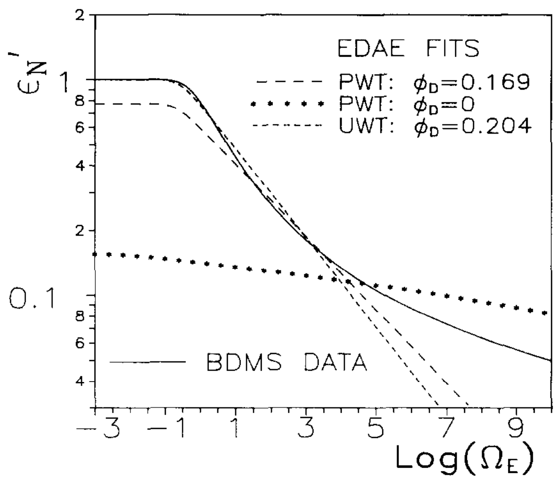

Fig. 16. ϵ'_N EDAE fit results vs. $\log(\Omega_E)$: * obtained with ϕ_D fixed at zero.

vation energies of the dc conductance and the CD relaxation time parameter were virtually identical, consistent with BDM response and a characteristic result for conducting system dispersion [7,20,25].

The present results indicate that since BDM model conducting system data can be much better fit at the ϵ level than can $\phi_D = 0$ EDAE dielectric system data at the complex modulus level, with reasonably good data one should usually be able to distinguish adequately between the possibilities, thus answering the question posed in Section 1 of distinguishing between the (c1) and (c2) types of response.

The conducting system bulk response need not involve only a frequency-independent resistance R_∞, and for most non-metallic non-superconducting materials it seems likely that it does not. Even for single crystals there is always some disorder at finite temperatures, and this disorder can and probably does lead to some frequency dispersion. Further, for reasonably high resistivity materials, the dispersion may occur within a measurable frequency region. For the BDM, the equations in the Appendix show that, when $\Omega_E = 1$ at $f = 10^6$ Hz,

$$\Delta Z'_C \equiv \Delta R_E \equiv (\epsilon_V/C_c)\Delta\rho'_E \approx 1.9 \times 10^{-5}/x_c C_c \quad (2)$$

where ϵ_V is the permittivity of vacuum. It is designated ϵ_V here rather than the more usual ϵ_0 or ϵ_o because these symbols may be confused with those denoting $\epsilon(0)$. Thus, with $x_c = 20$ and $C_c = 5 \times 10^{-12}$ F, $\Delta R_E \approx 2 \times 10^5$ Ω. A larger value of ΔR_E or x_c will cause the condition $\Omega_E = 1$ to occur at lower frequencies.

The presence of conducting system dispersion requires a nonzero $\Delta Z'_C$. Since the dispersion whose strength is defined by $\Delta Z'_C$ approaches zero at sufficiently high frequencies, there are two possibilities:

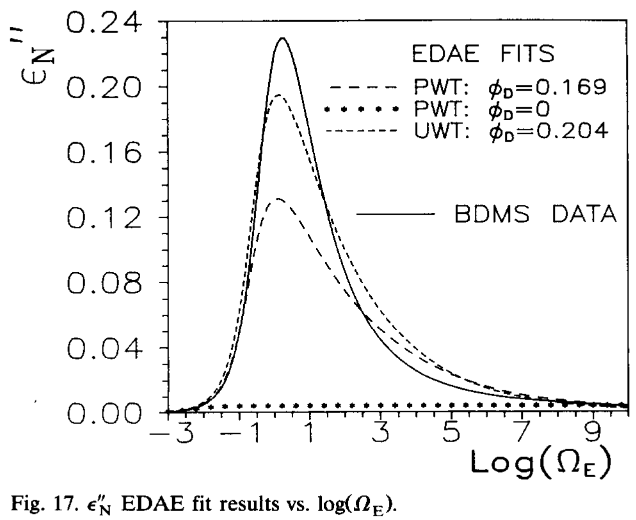

Fig. 17. ϵ''_N EDAE fit results vs. log(Ω_E).

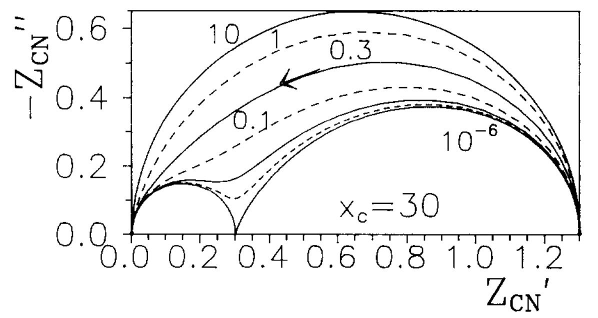

Fig. 18. Impedance complex-plane plots of Z_{CN} bulk response calculated using the BDM equation with $x_C = 30$. The numbers on each curve are values of $\epsilon'_{DN}(\infty)$, and the values for those between the curves for 0.1 and 10^{-6} are 0.03 and 0.01. Here $R_{\infty N} = 0.3$ and $\Delta Z'_{CN} = 1$.

either $Z'_C(\infty) \equiv R_{C\infty} \equiv R_\infty$ is zero or it is not. We begin by considering what might happen if it is not, a situation found to arise naturally for doped single-crystal NaCl [7].

Figure 18 shows some of the BDM response curve possibilities for an impedance-level complex plane plot with $R_{\infty N} = 0.3$, $\Delta Z'_{CN}$ necessarily equal to unity, and thus $Z'_C(0) = 1.3$. The curves are for different values of $\epsilon'_{DN}(\infty) \equiv \epsilon'_D(\infty)/\epsilon'_E(0)$, as listed on the figure and in the figure caption. Note the important difference in normalization here from that used in the dielectric system situation discussed above. The BDM quantity $\epsilon'_E(0)$ in the conducting system is defined in eqn. (A10). There are two apparent dispersions for very small $\epsilon'_{DN}(\infty)$ which meld into a single one for sufficiently large $\epsilon'_{DN}(\infty)$. When the effect of this quantity has been subtracted from the full data (by subtracting $i\Omega_E C'_{DN}(\infty)$ at the Y_N level), there will be no Debye semicircle between the limiting value $Z'_{CN}(\Omega_E) = R_{\infty N}$ and zero. In experimental situations where at least some of the small semicircle has been measured, the most appropriate value of $C'_{DN}(\infty)$ to subtract can be determined as that which yields the best approximation to zero Z''_{CN} response in the semicircle region. This will generally be the LEVM CNLS fit estimate also. It is important to emphasize that the two-arc result apparent for small $\epsilon'_{DN}(\infty)$ values in Fig. 18 is not composed of a bulk R_∞, C_∞ arc and an electrode reaction arc; both arcs here arise entirely from bulk behavior. One can distinguish between the two situations by making measurements for at least two different electrode separations of the measuring cell.

When the above subtraction has been carried out, one obtains the true dispersion shape associated with the dispersion process, here that of the BDM as in Fig. 11. It is clearly important to make this subtraction if one wishes to examine and possibly identify the true dispersion response of the material and not just the single-time-constant semicircle associated with R_∞ and C_∞. Further, we see that for intermediate values of $\epsilon'_{DN}(\infty)$, such as unity, the resultant curve is reasonably well approximated by a somewhat displaced semicircle, a result often found experimentally when, as usual, no subtraction is carried out [14,15,19].

In the second situation, $R_\infty \equiv 0$ and there is no possibility of two joined arcs. When the dispersion associated with $\Delta Z'_C I_C(\omega)$ occurs at frequencies beyond the upper limit of measurement, $\Delta Z'_C$ is likely to be confused with the frequency-independent quantity R_∞. Figure 19 shows how the actual dispersion can be hidden by the presence of C_∞ in this case. Here $\epsilon'_{DN}(\infty)$ varies from 10, where the true response is virtually completely hidden, to zero. Although the $\epsilon'_{DN}(\infty) = 10$ curve is a close approximation to single-time-constant response, at $\Omega_E = 1/10$, the expected peak frequency for this value, Z'_{CN} was 0.455 rather than 0.5 and $-Z''_{CN}$ was 0.496 rather than 0.5.

Figure 19 also includes an illustration of the subtraction process for n-GaAs single-crystal data at 400 K, normalized with respect to the measured value $Z'_C(0) \approx 1.7 \times 10^4$ Ω [41]. First, the unsubtracted data were fitted to the BDM equation using only three free parameters. The value of x_c employed was calculated from the estimate of the principal activation energy of the material in ref. 41. It was found that an adequate fit could only be obtained by allowing τ_E to be free, rather than by using its value from eqn. (A7). Orazem et al. [41] found a slightly better fit of these data with a different model using 11 free parameters. For a perfect fit, the present fit (asterisks) would fall at the center of the squares representing the actual data. If these data are actually well described by the present model, then the fit results yield a value of $\epsilon'_{DN}(\infty)$ of about 2.5.

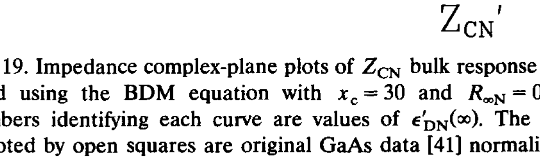

Fig. 19. Impedance complex-plane plots of Z_{CN} bulk response calculated using the BDM equation with $x_c = 30$ and $R_{\infty N} = 0$. The numbers identifying each curve are values of $\epsilon'_{DN}(\infty)$. The points denoted by open squares are original GaAs data [41] normalized to unity at dc. The asterisks near them are BDM equation fit results without subtraction of the effects of $\epsilon'_{DN}(\infty)$ estimated from the fit. For these result, $x_c \approx 23.4$. The open circles and the asterisks near them are the corresponding results after such subtraction.

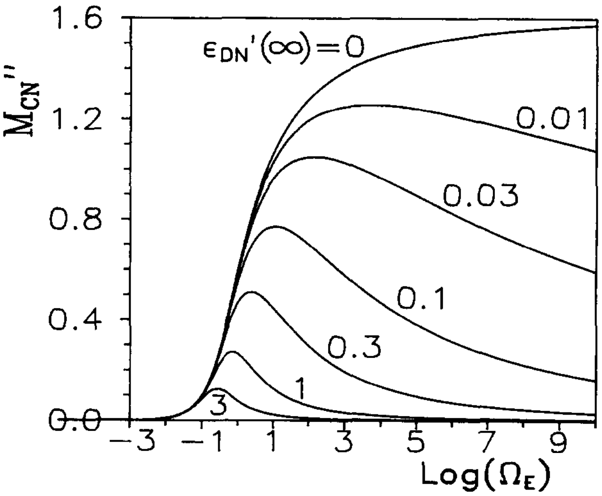

Fig. 20. M''_{CN} vs. $\log(\Omega_E)$ for the BDM with $x_c = 30$ showing the effect of nonzero $\epsilon'_{DN}(\infty)$.

Also shown in Fig. 19 are the normalized results of subtracting the effects of the fit estimate of $\epsilon'_D(\infty)$ from the GaAs data. The data after subtraction are indicated by open circles, and the BDM fit results of these data (with $\epsilon'_{DN}(\infty) = 0$) are shown by the asterisks nearby. Note that subtraction has increased the variability in the data, and that the fit results lie close to the BDM curve marked zero, as one would expect. It is unfortunate that the data obtained after subtraction do not extend to high enough frequencies to show whether the final response curve is indeed somewhat asymmetric, as it should be for the BDM response.

Figure 20 shows the M''_{CN} frequency response for the situation of Fig. 19. This figure, which should be compared with Fig. 5, shows that, in contrast with those results, nonzero $\epsilon'_{DN}(\infty)$ for a conducting system leads to asymmetric curve shapes which involve excess high frequency response: "endemic" behavior for amorphous polymers and molecular glasses according to ref. 30. The larger is $\epsilon'_{DN}(\infty)$ here, the closer the curves approach symmetry about their peaks and single-time-constant Debye behavior. The M''_{CN} curve for $\epsilon'_{DN}(\infty) = 0$ curve approaches the asymptotic value $\pi/2$ at high frequencies.

Finally, Figs. 21 and 22 show BDM model normalized complex modulus and complex resistivity results for three different temperatures with the following fixed typical values of the parameters in the Appendix: $E_c = 1.2$ eV and $\tau_{aE} = 3 \times 10^{-26}$ s. The frequency separation of the curves arises from the thermally activated behavior of the BDM relaxation time τ_E. In order to show the results for different temperatures on a single

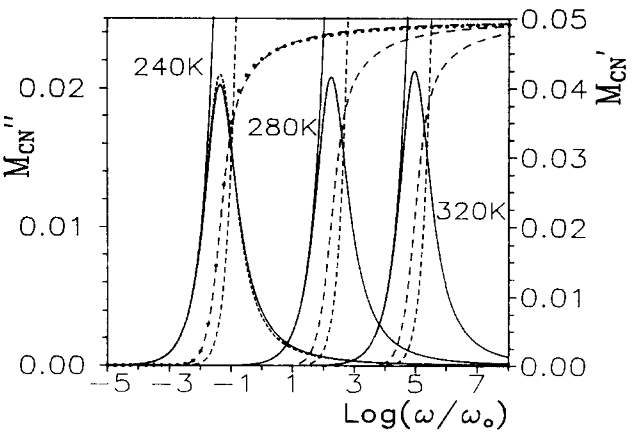

Fig. 21. M_{CN} BDM equation frequency dependence for three temperatures and the choices $\epsilon'_{DN}(\infty)=0$ and $\epsilon'_{DN}(\infty)=20$: M''_{CN} curves; ——— M'_{CN} curves. The $\epsilon'_{DN}(\infty)=0$ curves show neither peaks nor saturation. The 280 K peaked M''_{CN} curve (---) and the corresponding M'_{CN} curve (···) are EDAE fit results with ϕ_C fixed at unity and $x_H=60$. The normalizing quantity ω_0 is 1 rad s^{-1}.

graph with a linear scale, each data set was normalized by its dc resistivity value. These values were approximately 1.07×10^{13} Ω cm, 2.69×10^{9} Ω cm and 5.37×10^{6} Ω cm for 240 K, 280 K and 320 K, respectively. For both figures, results are shown with $\epsilon'_{DN}(\infty)$ values of zero and 20.

The real and imaginary curves of Fig. 21 show two characteristic features which are nearly always present in M-level plots for conducting system disordered-material response. These are the excess high frequency loss associated with the asymmetry of the M''_{CN} curves and the long approach to an asymptotic value at high frequencies exhibited by the M'_{CN} curves [6,8,30,31]. These curves approach the asymptotic value $[\epsilon'_{DN}(\infty)]^{-1}$ when this quantity is less than infinity, but the approach becomes very slow when $\epsilon'_{DN}(\infty)<1$. The asymptotic value of M'_C itself is just $[\epsilon'_D(\infty)]^{-1}$. But if there is no dielectric dispersion in the measured frequency range, one should replace $\epsilon'_D(\infty)$ by the possibly different quantity $\epsilon'_D(0)$ [20].

The EDAE box distribution conducting system fit results at 240 K of Fig. 21 are sufficiently close to those of the BDM for $\epsilon'_{DN}(\infty)=20$ that for most experimental data it would be difficult to distinguish between them. But, as Fig. 13 shows, when the effects of nonzero $\epsilon'_{DN}(\infty)$ have been subtracted from the data, there is sufficient difference in the responses to make discrimination possible for reasonably good data extending over five decades or more. Although the results of Fig. 21 show that there is a peak at the M_C level only when $\epsilon'_{DN}(\infty)\neq0$, those of Fig. 22 demonstrate that there is a peak at the impedance level whatever the value of this quantity. But with $\epsilon'_{DN}(\infty)=20$, the resulting curves are essentially R_∞, C_∞ single-time-constant curves, while both frequency response and shape are appreciably different for those with the effects of $\epsilon'_{DN}(\infty)$ removed.

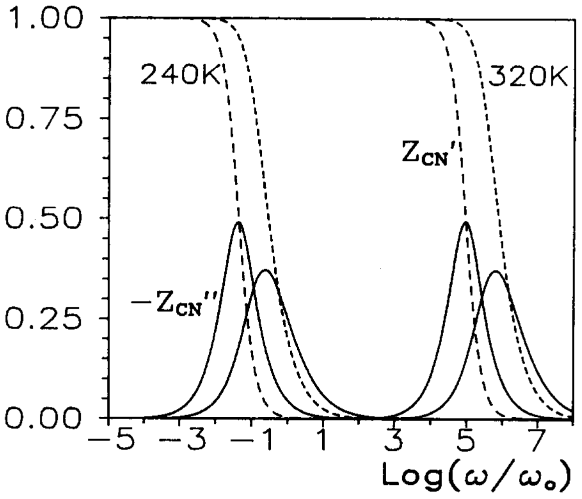

Fig. 22. Z_{CN} BDM equation frequency dependence for two temperatures and the choices $\epsilon'_{DN}(\infty)=0$ and $\epsilon'_{DN}(\infty)=20$. The leftmost curve of each pair is that with $\epsilon'_{DN}(\infty)=20$, and the other is for $\epsilon'_{DN}(\infty)=0$.

A few fits have been carried out to examine how well nonzero $\epsilon'_{DN}(\infty)$ values can be estimated from noisy data. Exact BDM Z-level data calculated with nonzero $\epsilon'_{DN}(\infty)$ values were truncated to three or two figures (excluding those defining the exponent). Thus a value such as 4.75912248×10^2 would become 4.7×10^2 with truncation to two figures. The results were fitted with the BDM with three free parameters using the LEVM CNLSF program. With three figures and $\epsilon'_{DN}(\infty)=20$, results were excellent: the standard deviation of the relative residuals of the fit was about 2×10^{-3} and an estimate of 20.04 was obtained. With two figures, the first figure was about 2.2×10^{-2} and the second about 20.5. Similarly, with $\epsilon'_{DN}(\infty)=400$, the value of 400.4 was obtained with three-figure accuracy and 408.2 ± 0.5 with two-figure data. Thus, for most experimental data, it should be possible to estimate $\epsilon'_D(\infty)$ adequately.

Appendix

In this Appendix the EDAE response model and the BDM conducting system response equation are briefly discussed. We follow earlier work by assuming that the transition rates of the system are thermally activated with a distribution of free-energy barriers [3,20,22–25]. For simplicity, assume that the distribution is in the activation energy E (actually enthalpy) only. Consider a thermally activated situation where a relaxation time τ_j is given by

$$\tau_j = \tau_{aj} \exp(E/k_B T) \tag{A1}$$

where $j = \mathrm{C}$ or D. Here τ_{aj}^{-1} is a barrier attempt frequency (usually 10^{12} Hz or greater), and the activation energy E satisfies $0 \le E \le E_H$. Further, define x_H as $E_H/k_B T$.

EDAE response

The EDAE equation, also termed a single exponential distribution of activation energies equation in past work [9,23,24], can be written in normalized form as

$$I_j(\Omega_H) \equiv \phi_j\left[1 - \exp(-\phi_j x_H)\right]^{-1} \times \int_0^{x_H} \frac{\exp(-\phi_j x)\,\mathrm{d}x}{1 + \mathrm{i}\Omega_H \exp(-x)} \tag{A2}$$

where

$$\Omega_H \equiv \omega\tau_H \tag{A3}$$

and τ_H is the value of τ_j from eqn. (A1) evaluated at $E = E_H$. The ϕ_j parameter is generally different from but related to the slope of the log–log admittance frequency response [23,24,26].

For the flat-top box distribution, $\phi_j \equiv \phi_C = 1$ for a conducting system and $\phi_D = 0$ for a dielectric system. For these and some other integral and fractional values of ϕ_j closed-form results can be found [22,23] from eqn. (A2). For example, for $\phi_j = 1$,

$$I(\Omega_H) = \frac{\ln\left[(1 + \mathrm{i}\Omega_H)/(1 + \mathrm{i}\Omega_H r^{-1})\right]}{(1 - r^{-1})\mathrm{i}\Omega_H} \tag{A4}$$

where $r \equiv \exp(x_H)$, and for $\phi_j = 0$ the result is

$$I(\Omega_H) = 1 - x_H^{-1} \ln\left[(1 + \mathrm{i}\Omega_H)/(1 + \mathrm{i}\Omega_H r^{-1})\right]. \tag{A5}$$

These results apply for either a conducting or a dielectric system: $I(\Omega_H)$ can then be defined as either a normalized impedance or a normalized complex dielectric constant respectively [23]. More results relating to the EDAE model are presented in refs. 3, 9 and 23–26.

BDM response

The derivation of this equation for a hopping situation has been discussed earlier [10,20]. One starts by averaging an effective-medium equation for the conductivity over a random free-energy-barrier probability distribution which is zero outside the E range defined above (a box distribution). The resulting equation for the conductivity, termed the GBEM equation in [20], involves $E_c \equiv E_H/3$ and $\tau_{aC} = \tau_{aE}$; it leads to a saturation value of Y_C' at very high frequencies and to a corresponding decrease in Y_C''. The subscript E is used here to distinguish the specific GBEM/BDM effective medium response from that of any other conducting system model. All the temperature dependence of GBEM response arises from that of the normalized maximum effective activation energy: $x_c \equiv E_c/k_B T$. The cross-over frequency f_{co}, where $Y_C' = Y_C''$, occurs at $f_{co} \approx 0.22(x_c\tau_{aE})^{-1}$, a frequency far above the frequency range of usual small-signal ac measurements.

The $T \to 0$ limit of the GBEM equation is the principal-value complex solution of the following implicit equation (the Bryksin equation [21]) for the normalized impedance quantity I_E of eqn. (1):

$$\ln(I_E) = -\mathrm{i}\Omega_E I_E \tag{A6}$$

where $\Omega_E \equiv \omega\tau_E$ is a normalized frequency variable. Consider the response expressed in terms of the complex resistivity $\rho_E(\Omega_E) \equiv (C_c/\epsilon_V)Z_E(\Omega_E)$ rather than the impedance. Then τ_E may be expressed as [20]

$$\tau_E = \Delta\rho_E'\epsilon_V\epsilon_E'(0)T_x \tag{A7}$$

In earlier work [10,20], $\epsilon_E'(0)$ was defined as the present $\epsilon_E'(0)$ times T_x, but this is merely a matter of definition. Temperature-dependent expressions for $\Delta\rho_E'$ and $\epsilon_E'(0)$ follow from the GBEM treatment [10,20]. They are

$$\Delta\rho_E' = (\tau_{aE}/\epsilon_V)R_x \tag{A8}$$

where

$$R_x \equiv 2\exp(x_c)/\left[1 + \exp(-x_c)\right] \tag{A9}$$

and

$$\epsilon_E'(0) \approx 0.0853 x_c \tag{A10}$$

Thus, although $\epsilon_E'(\infty) = 0$, there is a frequency-dependent dielectric level contribution from the present response for $\Omega_E < \infty$. The quantity $T_x \equiv 1$ for the GBEM.

Although GBEM response involves the solution of a much more complicated implicit equation than eqn. (A6), it has been found [10,20] that, for $f \ll f_{co}$, its normalized results are close to those of (A6) when eqns. (A7) and (A5) are used. In order to obtain a data-fitting equation which does not require the solution of an implicit equation for every frequency value, accurate $Y_N(\Omega_E)$ results calculated using the results of eqn (A6) and the GBEM response have been fitted with LEVM to an interpolating expression, the BDM equation [3,10,20,21,25]. To take adequate account of the response for $T \geqslant 0$ the BDM involves the choice

$$T_x = 1 - 1.5x_c^{-1} + \exp(-x_c) \tag{A11}$$

for $x_c \gtrsim 5$. For $x_c \to 0$, T_x approaches $x_c/4$.

The approximation error of the BDM in fitting both the $T \to 0$ limit of the GBEM and its $T > 0$ predictions is small compared with typical experimental errors provided that $f \ll f_{co}$. The BDM, whose expression involves many fixed fitting parameters, has been incorporated as a unified distributed circuit element in LEVM V. 6.1. Thus conducting system relaxation data can now be readily fitted using the BDM equation and the results interpreted in terms of the $\Delta\rho'_E$, $\epsilon'_E(0)$ and τ_E parameters defined above. When the value of x_c is known at a given temperature from the experimental conditions and temperature-dependent measurements of dc conductivity, x_c need not be a free fitting parameter. It is then usually most convenient to fit with $\Delta\rho'_E$ (or $\Delta Z'_E \equiv \Delta R_E$), $\epsilon'_D(0)$ and τ_E allowed to vary, and with R_∞ also a free fitting parameter when appropriate.

References

1 W.K. Lee, J.F. Liu and A.S. Nowick, Phys. Rev. Lett., 67 (1991) 1559.
2 B.S. Lim, A.V. Vaysleyb and A.S. Nowick, Appl. Phys., A 56, 8 (1993) (the citation to ref. 15 on p. 13 of this paper should be to ref. 16).
3 J.C. Dyre, Phys. Rev. B, 48 (1993) 12511.
4 A.R. Long, Adv. Phys., 31 (1982) 553.
5 S.R. Elliott, Adv. Phys., 36 (1987) 135.
6 P.-N. Huang and G.P. Johari, J. Mol. Liquids, 56 (1993) 225.
7 J.R. Macdonald, J. Appl. Phys., 75 (1994) 1059.
8 G.P. Johari and K. Pathmanathan, Phys. Chem. Glasses, 29 (1988) 219.
9 J.R. Macdonald and J.C. Wang, Solid State Ionics, 60 (1993) 319.
10 J.R. Macdonald, Appl. Phys. A, to be published.
11 R.L. Hurt and J.R. Macdonald, Solid State Ionics, 20 (1986) 111.
12 R.P. Buck and I. Krull, J. Electroanal. Chem. Interfacial Electrochem., 18 (1968) 387.
13 J.R. Sandifer and R.P. Buck, J. Electroanal. Chem. Interfacial Electrochem., 56 (1974) 385.
14 R.P. Buck, D.E. Mathis and R.K. Rhodes, J. Electroanal. Chem., 80 (1977) 245.
15 R.K. Rhodes and R.P. Buck, J. Electroanal. Chem., 86 (1978) 349.
16 J.R. Macdonald, J. Chem. Phys., 23 (1955) 275.
17 R.D. Armstrong, T. Dickinson and R. Whitefield, J. Electroanal. Chem., 39 (1972) 257.
18 R.D. Armstrong, T. Dickinson and P.M. Willis, J. Electroanal. Chem., 53 (1974) 389.
19 S. Lanyi and K. Hricovini, J. Phys. Chem. Solids, 44 (1983) 905.
20 J.R. Macdonald, Phys. Rev. B, 14 (1994) 9428.
21 V.V. Bryksin, Sov. Phys.-Solid State, 22 (1980) 1421.
22 A. Matsumoto and K. Higasi, J. Chem Phys., 36 (1962) 1776.
23 J.R. Macdonald, J. Appl. Phys., 58 (1985) 1955.
24 J.R. Macdonald, J. Appl. Phys., 61 (1987) 700.
25 J.C. Dyre, J. Appl. Phys., 64 (1988) 2456.
26 J.R. Macdonald, J. Appl. Phys., 65 (1989) 4845.
27 J.C. Wang and J.B. Bates, Solid State Ionics, 50 (1992) 75.
28 J.R. Macdonald and L.D. Potter Jr., Solid State Ionics, 23 (1987) 61.
29 J.R. Macdonald, Electrochim. Acta, 35 (1990) 1483.
30 C.T. Moynihan, L.P. Boesch and N.L. Laberge, Phys. Chem. Glasses, 14 (1973) 122.
31 F.S. Howell, R.A. Bose, P.B. Macedo and C.T. Moynihan, J. Phys. Chem., 78 (1974) 639.
32 J.R. Macdonald and M.N. Brachman, Rev. Mod. Phys., 28 (1956) 393.
33 J.R. Macdonald (Ed.), Impedance Spectroscopy-Emphasizing Solid Materials and Systems, Interscience, New York, 1987.
34 J.R. Macdonald, Electrochim. Acta, 38 (1993) 1883.
35 C.J.F. Bottcher and P. Bordewijk, Theory of Electronic Polarization, Vol. 2, Elsevier, Amsterdam, 1978, p. 47.
36 P. Agarwal and M.E. Orazem, J. Electrochem Soc., 139 (1992) 1917.
37 J.R. Macdonald and R.L. Hurt, J. Chem. Phys., 84 (1986) 496.
38 J.R. Macdonald and D.R. Franceschetti, J. Chem. Phys., 68 (1978) 1614.
39 K. Funke, Prog. Solid State Chem., 22 (1993) 111 (see Fig. 38).
40 R.H. Cole and E. Tombari, J. Non-Cryst. Solids, 131-133 (1991) 969.
41 M.E. Orazem, P. Agarwal, A.N. Jansen, P.T. Wojcik and L.H. Garcia-Rubio, Electrochim. Acta 38 (1993) 1903.